



## City Research Online

### City, University of London Institutional Repository

---

**Citation:** Pathak, A., Viphavakit, C., Rahman, B. M. & Singh, V. (2021). A Highly Sensitive SPR Refractive Index Sensor Based on Microfluidic Channel Assisted with Graphene-Ag Composite Nanowire. *IEEE Photonics Journal*, 13(2), pp. 1-8. doi: 10.1109/jphot.2021.3069396

This is the published version of the paper.

This version of the publication may differ from the final published version.

---

**Permanent repository link:** <https://openaccess.city.ac.uk/id/eprint/26145/>

**Link to published version:** <https://doi.org/10.1109/jphot.2021.3069396>

**Copyright:** City Research Online aims to make research outputs of City, University of London available to a wider audience. Copyright and Moral Rights remain with the author(s) and/or copyright holders. URLs from City Research Online may be freely distributed and linked to.

**Reuse:** Copies of full items can be used for personal research or study, educational, or not-for-profit purposes without prior permission or charge. Provided that the authors, title and full bibliographic details are credited, a hyperlink and/or URL is given for the original metadata page and the content is not changed in any way.

---

City Research Online:

<http://openaccess.city.ac.uk/>

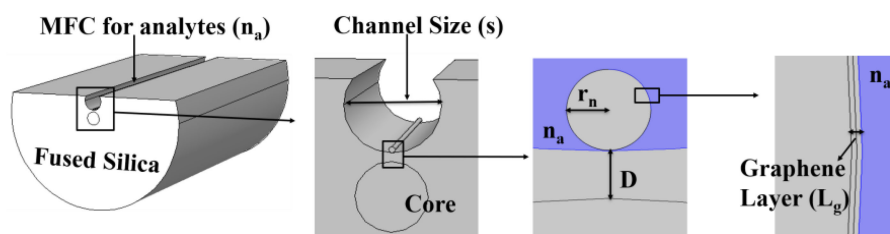
[publications@city.ac.uk](mailto:publications@city.ac.uk)

---

# A Highly Sensitive SPR Refractive Index Sensor Based on Microfluidic Channel Assisted With Graphene-Ag Composite Nanowire

Volume 13, Number 2, April 2021

Akhilesh K. Pathak  
Charusluk Viphavakit, *Member, IEEE*  
B. M. A. Rahman, *Life Fellow, IEEE*  
Vinod Kumar Singh, *Member, IEEE*



DOI: 10.1109/JPHOT.2021.3069396

# A Highly Sensitive SPR Refractive Index Sensor Based on Microfluidic Channel Assisted With Graphene-Ag Composite Nanowire

Akhilesh K. Pathak,<sup>1,2</sup> Charusluk Viphavakit<sup>1</sup>,<sup>1</sup> Member, IEEE,  
B. M. A. Rahman<sup>2</sup>,<sup>2</sup> Life Fellow, IEEE,  
and Vinod Kumar Singh,<sup>3</sup> Member, IEEE

<sup>1</sup>International School of Engineering (ISE), Intelligent Control Automation of Process Systems Research Unit, Chulalongkorn University, Bangkok 10330, Thailand

<sup>2</sup>School of Mathematics, Computer Science and Engineering, City University of London, London EC1V 0HB, U.K.

<sup>3</sup>Optical Fiber Laboratory, Indian Institute of Technology (Indian School of Mines), Dhanbad 826004, India

DOI:10.1109/JPHOT.2021.3069396

This work is licensed under a Creative Commons Attribution 4.0 License. For more information, see <https://creativecommons.org/licenses/by/4.0/>

Manuscript received February 23, 2021; revised March 22, 2021; accepted March 23, 2021. Date of publication March 29, 2021; date of current version April 14, 2021. This work was supported in part by the Second Century Fund (C2F), and Rachadapisek Sompote Fund for Intelligent Control Automation of Process Systems Research Unit, and for Development of New Faculty Staff (DNS 63\_088\_21\_005\_1), Chulalongkorn University. Corresponding author: Charusluk Viphavakit (e-mail: charusluk.v@chula.ac.th).

**Abstract:** A highly sensitive refractive index (RI) sensor based on a microfluidic channel (MFC) incorporated in a single-mode fiber (SMF), filled with Ag-graphene composite nanowire is presented and analyzed here. The sensing performance and the coupling properties of designed sensor are numerically analyzed by using a full vectorial finite element method (FEM) incorporating amplitude and wavelength interrogation techniques in the detection range varied from  $n_a = 1.330$ -1.350. The maximum wavelength and amplitude sensitivity are obtained of 13700 nm/RIU and 1026 RIU<sup>-1</sup>, respectively. Here, the Ag-graphene composite nanowire can not only solve the problem of oxidation but also enhances the sensitivity of the sensor. In addition of high sensitivity, it also provides better performance than other sensing devices based on similar technologies such as Ag nanowire-filled sensors. Moreover, the influences of polishing depth (D), nanowire radius ( $r_n$ ), graphene layer ( $L_g$ ) and channel size (s) on the designed sensor, are also thoroughly investigated here. The present work can provide a base for designing a real-time, highly sensitivity, remote sensing, and distributed SPR based RI sensor.

**Index Terms:** Microfluidic channel, nanowire, refractive index sensor, surface plasmon resonance.

## 1. Introduction

Surface plasmons are electromagnetic waves which arises due to the collective oscillation of the conduction electrons at the metal-dielectric interface, which is highly sensitive toward the changes in RI of analytes ( $n_a$ ). In 1992, Jorgenson *et al.*, proposed that an optical fiber can be used as a carrier to realize the surface plasmon resonance (SPR) phenomenon based on Kretschmann

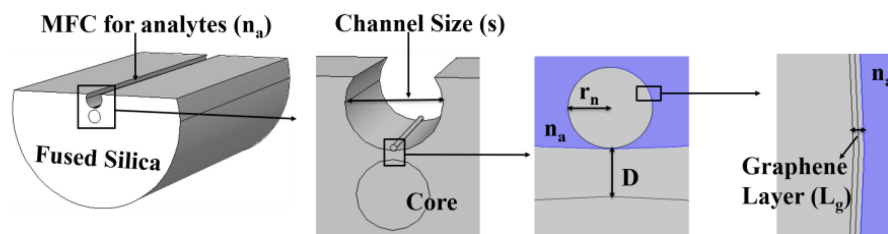


Fig. 1. Cross sectional view of designed sensor.

configuration [1], [2]. Based on this idea, various optical fiber SPR sensors are being fabricated and used widely in the investigation of RI measurement, biomolecular interaction analysis, health care, food safety, environmental monitoring, and homeland security [3]–[6].

In the optical fiber SPR sensors, gold (Au) and silver (Ag) have been widely used in various sensing areas due to the strong absorption property of these metals [7]. Compared to Au, Ag, one of the ideal metals shows the highest loss and sharper resonance peak for SPR with high detection accuracy, but Ag can be easily oxidized in the air [8]. In order to avoid the oxidation and improvement of the sensitivity, some additional materials e.g., graphene, are generally used on the surface of Ag [9]. Graphene is a 2D sheet of single-layer  $sp_2$ -bonded carbon atoms with a structure similar to the honeycomb lattice [10]. The SPR based optical fiber sensors using the graphene layer have been widely reported in past decades due to its high electron mobility, high surface volume ratio and strong absorption [11]. A fiber optic SPR sensor coated with  $TiO_2$  and graphene is reported by Patnaik *et al.* showing that the additional layer of graphene can enhance the sensitivity of the sensor distinctly and achieved a maximum sensitivity of 5700 nm/RIU [12]. Later Fu *et al.* improve the sensitivity by replacing the thin film coating by silver nanocolumn covered with the graphene layer and obtained an enhanced sensitivity of 8860 nm/RIU [13]. Therefore, a use of nanowire instead of the thin film can enhance the sensitivity but still a large amount of measurand for the detection is required. Optofluidic is a technique that integrates microfluidic with the optical system which can be used as the base of the RI sensor. The advantages of microfluidic system such as its configuration, size, sensing response and flexibility make it a potential candidate in various applications such as chemical detection, medical diagnostic, environmental monitoring, etc. [14]–[16]. The optical fiber-based optofluidic sensing configurations are simple and support low-cost fabrication support and also easy way for light to be coupled in and out of the chip and interacted with the liquid sample. Hence in this work, we have fully utilized the advantages of microfluidic technique along with the optical fiber to develop a refractive index sensor with improved sensitivity and for its possible fabrication realization.

In this paper, we report a highly sensitive optical fiber RI sensor using Ag-graphene composite nanowire. The sensor is analyzed by using the FEM technique. In order to achieve high sensitivity, we have performed a broad investigation on all the structural parameters such as separation of MFC from the core, nanowire radius, graphene layer and size of the MFC. Furthermore, we have also studied the fabrication tolerance of the designed sensor which may appear during the experimental realization. The sensitivity response of the sensor is calculated by wavelength and amplitude interrogation methods. The designed sensor with this high sensitivity can be useful in various chemical and biological sensing.

## 2. Structure and Theoretical Modeling

The schematic cross-sectional view of the designed sensor is shown in Fig. 1. The core/cladding diameter of the SMF is taken as  $9/125 \mu\text{m}$ , the radius of Ag nanowire is  $r_n = 0.25 \mu\text{m}$  and the polishing depth ( $D$ ) =  $0.3 \mu\text{m}$  is used here. As shown in Fig. 1, the analytes ( $n_a$ ) and graphene-Ag nanowire are placed inside the designed MFC of channel size ( $s$ ) =  $6 \mu\text{m}$ . Due to the gravity,

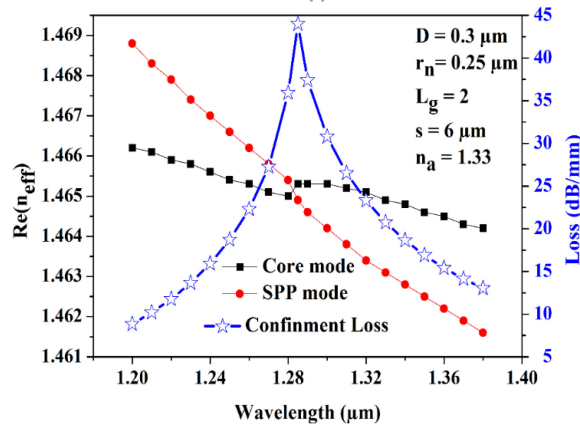


Fig. 2. Dispersion relation between the core-guided mode and the SPP mode at  $n_a = 1.33$ .

the composite nanowire sinks to the bottom of MFC and rests near the fiber core [17]. The bilayer coating of graphene is used here to avoid the oxidation of Ag nanowire and sensitivity enhancement [9]. Graphene's high electron density of hexagonal rings does not allow atoms as small as helium to penetrate it and it has a high surface to volume ratio which makes it a suitable candidate to be used as a functional coating material for currently available plasmonic instruments [18]. Every single layer of graphene has a thickness of 0.34 nm. The total thickness of the graphene layer ( $L_g$ ) is  $0.34 \text{ nm} \times L$ , where  $L$  is the number of graphene layers. The RI of graphene can be calculated by following relation [19].

$$n_g = 3 + (jC\lambda)/3 \quad (1)$$

where, where  $C \approx 5.446 \mu\text{m}^{-1}$  and  $\lambda$  represent the vacuum wavelength. The core and cladding of fiber are made of fused and Ge doped silica whose RI can be calculated by the Sellmeier equation [20] while the refractive index of Ag is calculated by using Lorentz-Drude model whose dielectric function can be defined as [21]

$$\varepsilon_m = 1 - \frac{\Omega_p^2}{\omega(\omega - i\Gamma_0)} + \sum_{j=1}^k \frac{f_j \omega_p^2}{(\omega_j^2 - \omega^2 + j\omega\Gamma_j)} \quad (2)$$

where,  $\varepsilon_m$  and  $\omega_p$  represent the dielectric constant and the plasma frequency whereas  $k$  is the number of oscillators with frequency  $\omega_p$  and strength  $f_j$ , while  $\Omega_p = \sqrt{f_0 \omega_p}$  shows the plasma frequency related with the intraband transition.

The designed sensor is analyzed by using full vectorial FEM. The modal analyses are performed in the XY plane while the light propagation is in the Z direction.

### 3. Results and Discussions

The dispersion relation between the dielectric core mode and surface plasmon polariton (SPP) mode is shown in Fig. 2. This plot illustrates that the real effective index ( $Re(n_{\text{eff}})$ ) of core and SPP modes at different wavelengths along with the confinement loss spectra of the designed SPR sensor. From Fig. 1 we can clearly observe that the  $Re(n_{\text{eff}})$  of SPP mode, shown by the red circle, decreases linearly while  $Re(n_{\text{eff}})$  of core mode, shown by the black circle remains nearly constant with the wavelength variation. The blue star exhibits the modal loss spectra at  $n_a = 1.33$ . The sensing performance measuring structural parameters of a designed sensor is estimated by using the confinement loss obtained for various analytes. Therefore, the confinement loss is a key factor

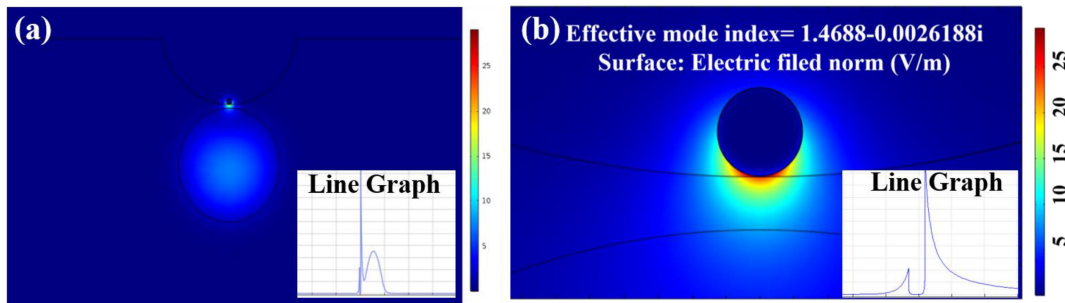


Fig. 3. (a) SPP mode electric field of the sensor. (b) Electric field around Ag-graphene composite nanowire. Insets are vertical field plot (y-axis).

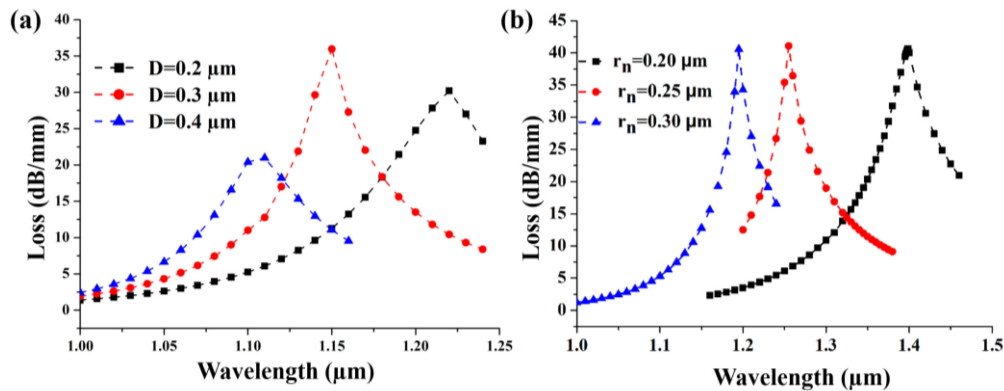


Fig. 4. (a) Variation of separation,  $D$ , from the core at  $r_n = 2 \mu\text{m}$ ,  $L_g = 1$  and  $s = 6 \mu\text{m}$ . (b) Variation of Ag nanowire diameter, at  $D = 0.3 \mu\text{m}$ ,  $L_g = 1$ , and  $s = 6 \mu\text{m}$ .

for the sensitivity measurement, and it can be calculated by following relation [17]

$$(\text{dB}/\text{m}) = 8.686k_0 \cdot \text{Im}(n_{\text{eff}}) \quad (3)$$

where the wavenumber ( $k_0$ ) is defined as  $k_0 = 2\pi/\lambda$  and  $\text{Im}(n_{\text{eff}})$  is known as the imaginary part of the effective index.

The SPP modes are very lossy in comparison to the dielectric core mode. So, when the core mode gets mixed with plasmonic mode close to the resonance wavelength ( $\lambda_R$ ), its loss value increased sharply, as shown by the blue dotted line. From the Fig. 2 we can clearly see that, as the wavelength increases, the energy transfer from dielectric core mode to plasmonic modes takes place and at  $\lambda_R = 1.285 \mu\text{m}$  the  $n_{\text{eff}}$  of these two modes becomes similar, which is known as resonance or phase-matching condition and form supermodes by coupling individual dielectric and plasmonic modes. At this position, the energy from the core mode is completely transferred to the plasmonic mode with a maximum loss of 43.98 dB/mm. Fig. 3(a) illustrates the mode profiles for SPP mode with the electrical field on y-axis as an inset. Fig. 3(b) illustrates the electric field around the Ag-graphene composite nanowire.

Fig. 4(a) illustrates the modal loss spectra of the fundamental mode corresponding to the various separation of MFC from the core. From this Fig. we can see that the maximum modal loss of 30.21 dB/mm, 35.95 dB/mm and 20.96 dB/mm are obtained for  $D = 0.2 \mu\text{m}$ ,  $0.3 \mu\text{m}$ , and  $0.4 \mu\text{m}$ , respectively. The maximum modal loss will lead the high response to the designed sensor hence  $D = 0.3 \mu\text{m}$  is chosen as an optimized separation of MFC from the core. In the numerical simulation, the separation ( $D$ ) of the MFC from the core plays a significant role in achieving the

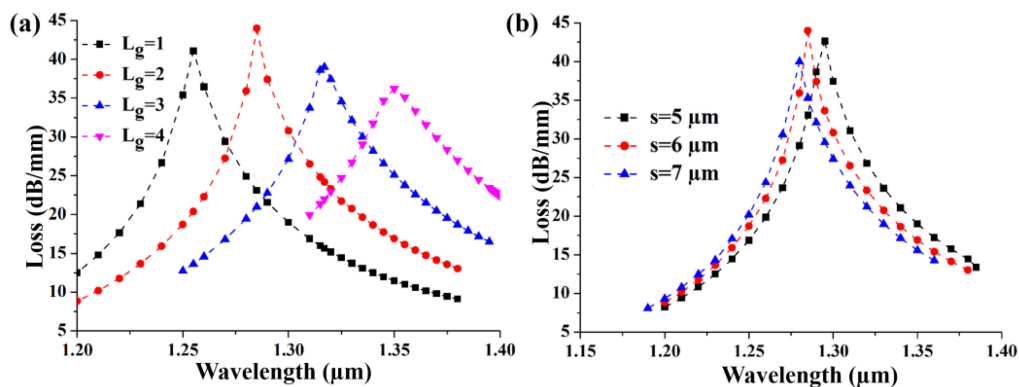


Fig. 5. (a) Variation in graphene layer,  $L_g$  over Ag nanowire, at  $D = 0.3 \mu\text{m}$ ,  $r_n = 0.25 \mu\text{m}$ , and  $s = 6 \mu\text{m}$ . (b) Variation of microfluidic channel size,  $s$ , at  $D = 0.3 \mu\text{m}$ ,  $r_n = 0.25 \mu\text{m}$  and  $L_g = 2$ .

maximum coupling between SPP and core modes. Hence before initiating the optimization of  $D$ , all other structural parameters such as  $r_n$ ,  $L_g$  and  $s$  are fixed while  $D$  is varied from  $0.2 \mu\text{m}$  to  $0.4 \mu\text{m}$ .

Fig. 4(b) illustrates the modal loss spectra of the fundamental mode with the variation of Ag nanowire radius ( $r_n$ ). The influence of  $r_n$  over the sensing performance can be clearly observed from Fig. 4(b). Before the optimization of  $r_n$ , all other structural parameters such as separation ( $D$ ), graphene layer ( $L_g$ ) and channel size ( $s$ ) are kept constant while nanowire radius ( $r_n$ ) is varied as  $0.20 \mu\text{m}$ ,  $0.25 \mu\text{m}$ , and  $0.30 \mu\text{m}$ . The maximum modal loss of  $40.65 \text{ dB/mm}$ ,  $41.07 \text{ dB/mm}$ , and  $40.58 \text{ dB/mm}$  are obtained for nanowire radius of  $0.20 \mu\text{m}$ ,  $0.25 \mu\text{m}$ , and  $0.30 \mu\text{m}$ , respectively with good redshift in loss spectra.

Fig. 5(a) shows the loss spectra of the sensor when the graphene layers ( $L_g$ ) on Ag nanowire is varied from  $L_g = 1$  to 4 in the step of 1 layer. With increase in  $L_g$  the blue shifts significantly occurs in resonance wavelength, also the peak loss value decreases considerably as the dielectric core mode becomes isolated from the SPP occurs due to the limited penetration of the core mode, then the coupling between the SPP and core mode will weaken, leads the low coupling and hence lower peak loss. From this Fig. we can clearly observe a maximum loss of  $43.98 \text{ dB/mm}$  for bilayer coating of graphene over Ag-nanowire.

Next, the role played by the size of MFC is also considered for analyzing the sensing performance of the designed sensor. Fig. 5(b) exhibits the variation in loss spectra with the channel size. It can be seen from Fig. 5(b), the maximum modal loss of  $43.98 \text{ dB/mm}$  is obtained for  $s = 6 \mu\text{m}$ , while for modal loss for MFC of size  $5 \mu\text{m}$  and  $7 \mu\text{m}$  are  $42.65 \text{ dB/mm}$  and  $39.98 \text{ dB/mm}$ , respectively. This maximum loss for  $s = 6 \mu\text{m}$  may takes place due to the fact that far from the core of the fiber, the interaction region of the electric field of core guided mode with the metal-dielectric interface is more due to the expansion of the electric field. As the channel size increases or decreases from its optimized values the interaction get smaller and also the loss. Moreover, when the metal-dielectric interface is far from the core, the field strength becomes weaken and result in the least modal loss. A smaller size is convenient as a sensor, i.e., due to its small size, it requires only a small amount of analyte for the measurement.

Considering all the above numerical analyses, we have kept the structural parameters e.g.,  $D = 0.3 \mu\text{m}$ ,  $r_n = 0.25 \mu\text{m}$ ,  $L_g = 2$  and  $s = 6 \mu\text{m}$ , respectively for the characterization of this RI sensor. Fig. 6(a) illustrates the modal loss variation with respect to various  $n_a$ . Here, we can clearly observe that when the  $n_a$  is varied from  $1.330$  to  $1.350$  at a step of  $0.005$ , the strong blue shift occurs in resonance wavelength varied from  $1.285 \mu\text{m}$  to  $1.560 \mu\text{m}$ . This blue shift occurs due to the change in  $\text{Re}(n_{\text{eff}})$  of SPP mode. Fig. 6(b) shows the amplitude sensitivity of the designed sensor. For some specific wavelength, the sensitivity of the sensor can be measured by using the

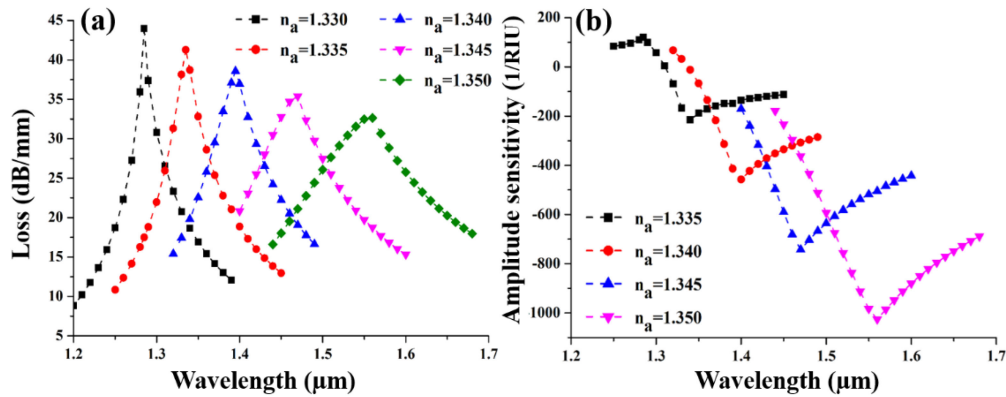


Fig. 6. (a) Variation in Loss spectrum and (b) amplitude sensitivity of the designed sensor with variation of  $n_a$ , At optimized parameters  $D = 0.3 \mu\text{m}$ ,  $r_n = 0.25 \mu\text{m}$ ,  $L_g = 2$  and  $s = 6 \mu\text{m}$ .

TABLE 1

Sensitivity Comparison of Present Work With Previously Reported Work

References	Wavelength sensitivity (nm/RIU)	Amplitude sensitivity (RIU <sup>-1</sup> )
[22]	4600	420
[23]	5000	167
[24]	10000	249
[25]	10700	-
[26]	12000	1086
Our work	13700	1026

amplitude interrogation technique and can be defined as [22].

$$S_A (\text{RIU}^{-1}) = -\frac{1}{\alpha(\lambda, n_a)} \cdot \frac{\partial \alpha(\lambda, n_a)}{\partial n_a} \quad (4)$$

where,  $\alpha(\lambda, n_a)$  is defined as the modal loss value for any analytes ( $n_a$ ) and  $\partial \alpha(\lambda, n_a)$  is the modal loss difference for  $n_a$ . According to the Fig. 6(b), we can observe that the amplitude sensitivity goes higher as we increase  $n_a$ . Higher  $n_a$  value depicts the stronger interaction between the SPP and core guided mode, which results in the dramatic increase in amplitude sensitivity. The maximum sensitivities are obtained of 215, 457, 742 and 1/1026 RIU, respectively, with respect to the  $n_a$  of 1.335, 1.340, 1.345, 1.350, respectively. Moreover, a maximum  $S_A$  of 1026 RIU<sup>-1</sup> for the measurement of analytes of  $n_a = 1.350$  can be achieved.

The variation in resonance wavelength ( $\lambda_{peak}$ ) corresponding to analytes ( $n_a$ ) varied from 1.330 to 1.350 can be used to calculate for the sensitivity of the sensor;

$$S_\lambda = \frac{\Delta \lambda_{peak}}{\Delta n_a} \quad (\text{nm/RIU}) \quad (5)$$

where  $S_\lambda$  and  $\Delta \lambda_{peak}$  are the sensitivity and resonance wavelength shift, respectively.  $\Delta n_a$  is the change in RI of analytes.

A maximum wavelength sensitivity of 13700 nm/RIU is obtained for the  $n_a$  ranges from 1.33 to 1.35 with a strong linear relation of 0.98. Table 1 shows the sensitivity comparison of the previously reported work with this work.

#### 4. Fabrication and Tolerance Investigation

In general, a small variation of  $\pm 1\%$  can occur in the optimized structural parameters during the fabrication. To validate the reported performance of the designed sensor, we have investigated

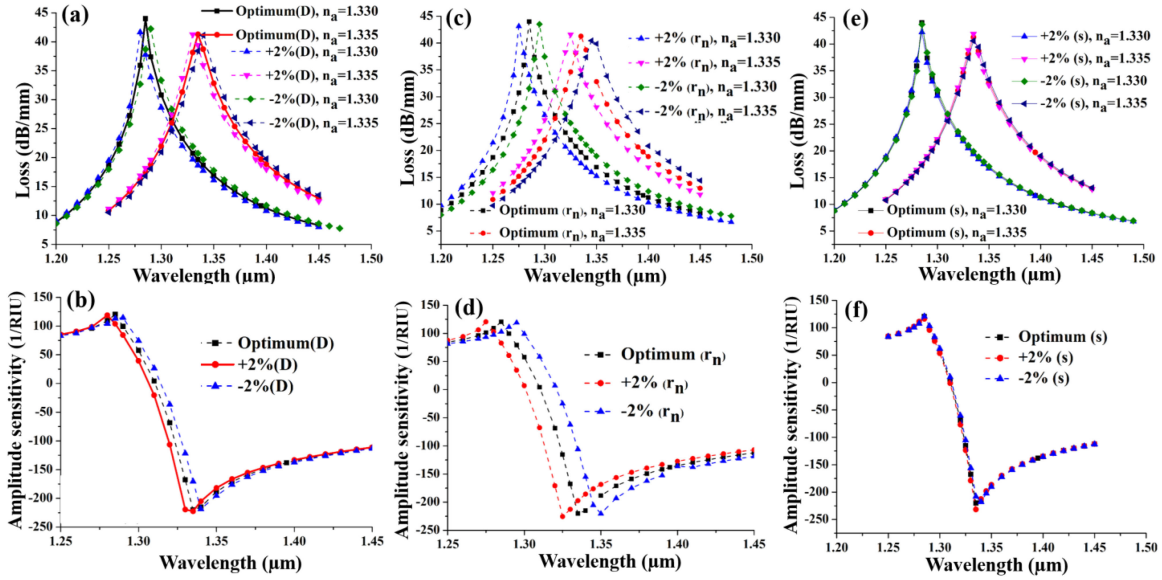


Fig. 7. Loss spectra due to  $\pm 2\%$  variation (a) in MFC separation,  $D$ , (c) in nanowire radius,  $r_n$ , and (e) in channel size,  $s$ . Amplitude sensitivity due to  $\pm 2\%$  variation (b) in MFC separation,  $D$ , (d) in nanowire radius,  $r_n$ , and (f) in channel size,  $s$ .

the proposed structural parameter with the fabrication tolerance of  $\pm 2\%$ . Fig. 7(a) illustrates the influence of MFC separation ( $D$ ) on loss spectra with the variation of  $\pm 2\%$  from its optimum value. It is clearly seen that the loss decreases to 41.64 dB/mm and 42.24 dB/mm from its optimum value of 43.98 dB/mm, due to  $+2\%$  and  $-2\%$  variation in  $D$ , respectively, at the  $n_a = 1.330$ . For  $n_a = 1.335$ , the tolerance variation of  $\pm 2\%$   $D$ , the measured loss is obtained of 41.25 dB/mm and 41.17 dB/mm whereas, the optimum loss value was observed of 41.26 dB/mm. The amplitude sensitivity corresponding to this variation is plotted in Fig. 7(b) which can be seen that the maximum amplitude sensitivity is increased by  $2.52 \text{ RIU}^{-1}$  and decreased by  $1.53 \text{ RIU}^{-1}$  due to  $\pm 2\%$  variation of  $D$ .

Additionally, the loss spectra due to  $\pm 2\%$  variation of nanowire radius  $r_n$  is presented in Fig. 7(c). The spectral loss is decreased by 0.878 dB/mm and 0.46 dB/mm due to  $+2\%$  and  $-2\%$  variation of  $r_n$  from their optimum value at 43.98 dB/mm at  $n_a = 1.330$  and for  $n_a = 1.335$  the loss value decreased by 2.41 dB/mm and 3.53 dB/mm due to  $\pm 2\%$  variation of  $r_n$ . The maximum amplitude sensitivity is increased by  $5.58 \text{ RIU}^{-1}$  and  $0.38 \text{ RIU}^{-1}$  for  $+2\%$  and  $-2\%$ , respectively from its optimum value  $220 \text{ RIU}^{-1}$  as shown in Fig. 7(d). Although, this variation leads to the change in its sensitivity, but the changes are very small hence it could be a realistic approach for the proposed sensor.

Furthermore, the influence of variation of channel size ( $s$ ) on loss spectra is shown in Fig. 7(e). It can be seen that, for  $n_a = 1.330$ , the modal loss spectra decrease to 42.23 dB/mm and 43.63 dB/mm from its optimum value 43.98 dB/mm. In case of  $n_a = 1.335$ , the loss spectra decrease to 41.89 dB/mm and 40.59 dB/mm from its optimum value of 43.98 dB/mm. It can be noticed that almost resonance wavelengths almost remain the same throughout the variation of  $\pm 2\%$  of  $s$ , respectively, for both  $n_a$ . Therefore, just like  $D$  and  $r_n$ , the  $\pm 2\%$  variation of  $s$  leads to a small variation in amplitude. According to Fig. 7(f), the  $+2\%$  increment of  $s$ , the amplitude sensitivity is increased by  $11.52 \text{ RIU}^{-1}$  and is decreased by  $2.28 \text{ RIU}^{-1}$  due to  $-2\%$  decrement. Hence, we can say that the  $\pm 2\%$  variation in its structural parameter will not affect its sensitivity, during the experimental realization.

## 5. Conclusion

Ag-graphene composite nanowire filled in MFC incorporated in SMF is presented and analyzed in this paper for a highly sensitive SPR based RI sensor. The advantage of the graphene layer is to prevent Ag nanowire from oxidation and sensitivity enhancement. Moreover, the graphene layer also enables the designed sensor for biomolecules. The sensor is analyzed and characterized using the FEM technique. The performance of the designed sensor is analyzed in terms of wavelength and amplitude sensitivity with a maximum sensitivity of 13700 nm/RIU and 1026 RIU<sup>-1</sup>, respectively. The small size and high sensitivity make the sensor a promising candidate for low and high refractive indices chemical and the additional layer of graphene makes it eligible for biosensing too

## References

- [1] R. C. Jorgenson and S. S. Yee, "A fiber-optic chemical sensor based on surface plasmon resonance," *Sensors Actuators B: Chem.*, vol. 12, pp. 213–220, 1993.
- [2] E. Kretschmann and H. Raether, "Notizen: Radiative decay of non radiative surface plasmons excited by light," *Zeitschrift Für Naturforsch. A.*, vol. 23, pp. 2135–2136, 1968.
- [3] B. Prabowo, A. Purwidyantri, and K.-C. Liu, "Surface plasmon resonance optical sensor: A review on light source technology," *Biosensors*, vol. 8, 2018, Art. no. 80.
- [4] C. Viphavakit, S. O. Keeffe, M. Yang, S. Andersson-Engels, and E. Lewis, "Gold enhanced hemoglobin interaction in a fabry-pérot based optical fiber sensor for measurement of blood refractive index," *J. Lightw. Technol.*, vol. 36, pp. 1118–1112, 2018.
- [5] H. Fu *et al.*, "TCF-MMF-TCF fiber structure based interferometer for refractive index sensing," *Opt. Lasers Eng.*, vol. 69, pp. 58–61, 2015.
- [6] P. Dhara *et al.*, "Optical fiber-based heavy metal detection using the localized surface plasmon resonance technique," *IEEE Sensors J.*, 2019, vol. 19, no. 19, pp. 8720–8726, Oct. 2019.
- [7] S. Kumari and S. Gupta, "Performance estimation of hybrid plasmonic waveguide in presence of stress," *Plasmonics*, vol. 16, pp. 359–370, 2020.
- [8] H. Fu, S. Zhang, H. Chen, and J. Weng, "Graphene enhances the sensitivity of fiber-optic surface plasmon resonance biosensor," *IEEE Sensors J.*, vol. 15, pp. 5478–5482, 2015.
- [9] Y. Saad, M. Selmi, M. H. Gazzah, and H. Belmabrouk, "Graphene effect on the improvement of the response of optical fiber SPR sensor," *IEEE Sensors J.*, vol. 17, pp. 7440–7447, 2017.
- [10] T. Zhang, S. Wu, R. Yang, and G. Zhang, "Graphene: Nanostructure engineering and applications," *Front. Phys.*, vol. 12, 2017, Art. no. 127206.
- [11] J. A. Kim *et al.*, "Graphene based fiber optic surface plasmon resonance for bio-chemical sensor applications," *Sensors Actuators B: Chem.*, vol. 187, pp. 426–433, 2013.
- [12] A. Patnaik, K. Senthilnathan, and R. Jha, "Graphene-based conducting metal oxide coated D-shaped optical fiber SPR sensor," *IEEE Photon. Technol. Lett.*, vol. 27, pp. 2437–2440, 2015.
- [13] H. Fu *et al.*, "A high sensitivity D-type surface plasmon resonance optical fiber refractive index sensor with graphene coated silver nano-columns," *Opt. Fiber Technol.*, vol. 48, pp. 34–39, 2019.
- [14] Z. Yang, L. Xia, S. Li, R. Qi, X. Chen, and W. Li, "Highly sensitive refractive index detection based on compact HSC-SPR structure in a microfluidic chip," *Sensors Actuators A: Phys.*, vol. 297, 2019, Art. no. 111558.
- [15] H. Zhang, P. Palit, Y. Liu, S. Vaziri, and Y. Sun, "Reconfigurable integrated optofluidic droplet laser arrays," *ACS Appl. Mater. Interfaces.*, vol. 12, pp. 26936–26942, 2020.
- [16] H. Zhang, C. Zhang, S. Vaziri, F. Kenarangi, and Y. Sun, "Microfluidic ionic liquid dye laser," *IEEE Photon. J.*, vol. 13, 2021, Art. no. 1500308.
- [17] A. K. Pathak, and V. K. Singh, "SPR based optical fiber refractive index sensor using silver nanowire assisted CSMFC," *IEEE Photon. Technol. Lett.*, vol. 32, pp. 465–468, 2020.
- [18] Y. Zhao, X. Li, X. Zhou, and Y. Zhang, "Review on the graphene based optical fiber chemical and biological sensors," *Sensors Actuators B: Chem.*, vol. 231, pp. 324–340, 2016.
- [19] H. Liang, T. Shen, Y. Feng, H. Liu, and W. Han, "A D-Shaped photonic crystal fiber refractive index sensor coated with graphene and zinc oxide," *Sensors*, vol. 21, 2020, Art. no. 71.
- [20] V. Brucker, *To the Use of Sellmeier Formula*. Germany: Springer, 2011.
- [21] A. D. Rakić, A. B. Djurišić, J. M. Elazar, and M. L. Majewski, "Optical properties of metallic films for vertical-cavity optoelectronic devices," *Appl. Opt.*, vol. 37, 1998, Art. no. 5271.
- [22] M. R. Hasan *et al.*, "Spiral photonic crystal fiber-based dual-polarized surface plasmon resonance biosensor," *IEEE Sensors J.*, vol. 18, pp. 133–140, 2018.
- [23] J. N. Dash, R. Das, and R. Jha, "AZO coated microchannel incorporated PCF-Based SPR sensor: A numerical analysis," *IEEE Photon. Technol. Lett.*, vol. 30, pp. 1032–1035, 2018.
- [24] M. A. Khalek, S. Chakma, K. Ahmed, B. K. Paul, D. Vigneswaran, and R. Zakaria, "Materials effect in sensing performance based on surface plasmon resonance using photonic crystal fiber," *Plasmonics*, vol. 14, pp. 861–867, 2019.
- [25] Z. Yang, L. Xia, C. Li, X. Chen, and D. Liu, "A surface plasmon resonance sensor based on concave-shaped photonic crystal fiber for low refractive index detection," *Opt. Commun.*, vol. 430, pp. 195–203, 2019.
- [26] M. Al Mahfuz *et al.*, "Highly sensitive photonic crystal fiber plasmonic biosensor: Design and analysis," *Opt. Mater. (Amst.)*, vol. 90, pp. 315–321, 2019.